

# CHANDRA STACKING CONSTRAINTS ON THE CONTRIBUTION OF 24 MICRON *SPITZER* SOURCES TO THE UNRESOLVED COSMIC X-RAY BACKGROUND.

A. T. STEFFEN<sup>1</sup>, W. N. BRANDT<sup>1</sup>, D. M. ALEXANDER<sup>2</sup>, S. C. GALLAGHER<sup>3</sup>, B. D. LEHMER<sup>1</sup>

Submitted to *ApJ Letters*, 2007 May 14

## ABSTRACT

We employ X-ray stacking techniques to examine the contribution from X-ray undetected, mid-infrared-selected sources to the unresolved, hard (6–8 keV) cosmic X-ray background (CXB). We use the publicly available, 24 $\mu$ m *Spitzer Space Telescope* MIPS catalogs from the Great Observatories Origins Deep Survey (GOODS) - North and South fields, which are centered on the 2 Ms *Chandra* Deep Field-North and the 1 Ms *Chandra* Deep Field-South, to identify bright ( $S_{24\mu\text{m}} > 80\mu\text{Jy}$ ) mid-infrared sources that may be powered by heavily obscured AGNs. We measure a significant stacked X-ray signal in all of the X-ray bands examined, including, for the first time, a significant ( $3.2\sigma$ ) 6–8 keV stacked X-ray signal from an X-ray undetected source population. We find that the X-ray-undetected MIPS sources make up about 2% (or less) of the total CXB below 6 keV, but about 6% in the 6–8 keV band. The 0.5–8 keV stacked X-ray spectrum is consistent with a hard power-law ( $\Gamma = 1.44 \pm 0.07$ ), with the spectrum hardening at higher X-ray energies. Our findings show that these bright MIPS sources do contain obscured AGNs, but are not the primary source of the unresolved 50% of 6–8 keV CXB. Our study rules out obscured, luminous QSOs as a significant source of the remaining unresolved CXB and suggests that it most likely arises from a large population of obscured, high-redshift ( $z \gtrsim 1$ ), Seyfert-luminosity AGNs.

*Subject headings:* Galaxies: Active: Nuclei — Galaxies: Active: Infrared/X-ray — X-rays: Diffuse Background

## 1. INTRODUCTION

Deep “blank-sky” surveys with the *Chandra X-ray Observatory* (hereafter *Chandra*) have resolved  $\sim 50$ – $90\%$  of the hard (2–8 keV) cosmic X-ray background (CXB) into discrete sources (e.g., Bauer et al. 2004; De Luca & Molendi 2004; Hickox & Markevitch 2006), with the resolved fraction decreasing with increasing X-ray energy (Worsley et al. 2004, 2005). Subsequent spectroscopic observations have revealed that the majority of the sources are Active Galactic Nuclei (AGNs; e.g., Barger et al. 2003; Steffen et al. 2004; Szokoly et al. 2004). This is consistent with CXB synthesis models, which rely on the assumptions of the “unified” AGN model (see Antonucci 1993, for a review), that predict the observed power-law ( $\Gamma \simeq 1.4$ ) shape of the CXB is created by the integrated X-ray emission from both soft ( $\Gamma \sim 1.8$ ), unobscured and harder ( $\Gamma < 1.4$ ), obscured<sup>4</sup> AGNs (e.g., Comastri et al. 1995; Gilli et al. 2007).

Although deep X-ray surveys find the highest sky density of AGNs to date ( $\sim 7000 \text{ deg}^{-2}$ ; Bauer et al. 2004), the decreasing resolved fraction of the CXB with energy suggests that there exists an additional, highly-obscured AGN population that is missed in even the deepest X-ray surveys (Worsley et al. 2005). While the majority of the X-ray emission from these sources is attenuated, a small fraction of hard X-ray photons can penetrate the obscuring torus. In addition, hard (rest-frame  $> 10$  keV) X-ray emission can be scattered into the observer’s line-of-sight via Compton reflection, which comprises a relatively larger fraction of the total observed X-ray emission from a heavily obscured AGN. The fraction

of hard X-ray photons emitted from a heavily obscured source would likely be too small to identify the source individually, but the hard X-ray emission from many of these undetected, Compton-thick sources could comprise the unresolved CXB.

Since the absorbed energy in obscured AGNs is re-emitted in the mid- and far-infrared, obscured AGNs should be bright *Spitzer* sources. The dust reprocessing of AGN accretion energy heats the dust to higher temperatures than can be achieved by heating via stellar processes, and this emission appears to be relatively isotropic (Lutz et al. 2004). The strong rest-frame 3–8 $\mu$ m thermal continuum produced by the AGN-heated dust can be used to separate luminous AGNs from starbursts using infrared color-color selection (Laurent et al. 2000; Lacy et al. 2004; Stern et al. 2005) and infrared power-law selection (Alonso-Herrero et al. 2006; Donley et al. 2007). Once candidate AGNs have been identified, X-ray stacking analyses can be used to measure their average X-ray properties and determine their contribution to the CXB below the detection limit of individual X-ray sources.

In this Letter, we use X-ray stacking techniques to examine the contribution of MIPS-detected GOODS sources to the unresolved component of the CXB. In §2 we describe the X-ray and infrared data used in this study. Our analyses are presented in §3. Our discussion and conclusions are in §4. We use the cosmological parameters  $H_0 = 70 \text{ km s}^{-1} \text{ Mpc}^{-1}$ ,  $\Omega_M = 0.3$ , and  $\Omega_\Lambda = 0.7$ .

## 2. SAMPLE

The 2 Ms *Chandra* Deep Field-North and 1 Ms *Chandra* Deep Field-South are currently the deepest 0.5–8 keV surveys (Giacconi et al. 2002; Alexander et al. 2003). The high spatial resolution of *Chandra* ( $\sim 0''.5$  at the aimpoint) and *Chandra*’s low background make these images ideal for examining the resolved fraction of the CXB. We use the X-ray catalogs of Alexander et al. (2003) for both the CDF-N and CDF-S, which contain 503 and 326 X-ray sources, respec-

<sup>1</sup> Department of Astronomy and Astrophysics, 525 Davey Laboratory, Pennsylvania State University, University Park, PA 16802.

<sup>2</sup> Department of Physics, University of Durham, South Road, Durham, DH1 3LE, UK.

<sup>3</sup> Department of Physics and Astronomy, University of California, 430 Portola Plaza, Box 951547 Los Angeles CA, 90095-1547.

<sup>4</sup> The term ‘obscured’ refers to X-ray obscuration, unless otherwise noted.

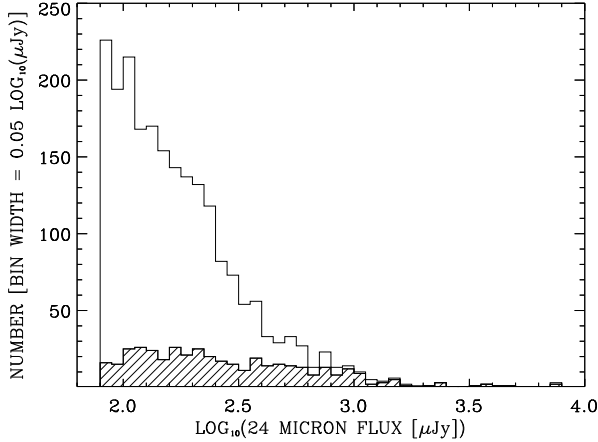


FIG. 1.— Histogram of  $24\mu\text{m}$  fluxes for the 2147 MIPS-selected sources in the GOODS-North & South fields (*open histogram*). The  $24\mu\text{m}$  flux distribution of MIPS sources with X-ray counterparts is shown for comparison (*hatched histogram*).

tively, detected using *wavdetect* at a significance threshold of  $10^{-7}$ . We also consider the supplementary X-ray source catalogs for both fields, which add an additional 79 (42) sources to the CDF-N (CDF-S); these sources are detected with a looser threshold ( $10^{-5}$ ), but because they are coincident with optically bright ( $R < 23$ ) sources, the vast majority ( $> 90\%$ ) are likely real.

To identify obscured AGN candidates, we use *Spitzer* data from the Great Observatories Origins Deep Survey (GOODS; Dickinson & GOODS Team 2005). The GOODS infrared catalogs consist of observations in the four IRAC bands (3.6, 4.5, 5.8, and  $8.0\mu\text{m}$ ; Fazio et al. 2004) and one MIPS band ( $24\mu\text{m}$ ; Rieke et al. 2004). The contribution to the CXB from the IRAC-selected sources will be presented in a subsequent paper (Steffen et al. 2007, in prep). In this Letter we measure the contribution of the MIPS sources to the CXB.

The GOODS MIPS observations are publicly available<sup>5</sup> as part of GOODS data releases DR1 (GOODS-North) and DR3 (GOODS-South). The GOODS-North and GOODS-South MIPS-selected catalogs contain 1199 and 948 sources, respectively, extending down to a  $24\mu\text{m}$  flux limit of  $\sim 80\mu\text{Jy}$ . We cross-correlated the MIPS source positions with the aforementioned X-ray catalogs using a  $3''$  matching radius. We found 253 (156) CDF-N (CDF-S) MIPS sources matched to an X-ray counterpart within  $3''$  (with an expectation of  $\sim 20$  spurious matches). In Figure 1, we present histograms showing the distribution of  $24\mu\text{m}$  fluxes for all MIPS-selected GOODS sources (*open histogram*) and for the MIPS sources with X-ray counterparts (*hatched histogram*). It is apparent that while the number of MIPS sources increases at fainter fluxes, the number of sources with X-ray counterparts increases slowly, so the fraction of MIPS sources with a detected X-ray counterpart decreases as one examines fainter  $24\mu\text{m}$  MIPS sources. This is consistent with the idea that luminous AGNs power the brightest  $24\mu\text{m}$  sources, while the fainter sources can be powered by the more common dusty starbursts.

### 3. ANALYSIS

We used X-ray stacking techniques to examine the contribution of MIPS-selected AGN candidates to the unresolved

CXB. We calculated the total number of photons within a  $3''$  diameter circular aperture, correcting for the fractional contribution from pixels only partially covered by the aperture. The local background is measured by extracting the total number of counts within a  $30\text{ pixel} \times 30\text{ pixel}$  ( $\sim 15'' \times 15''$ ) box, centered on a source and masking all of the known X-ray and MIPS source positions.

To calculate the expected background in the desired aperture, the total number of background counts is scaled by the ratio of the summed exposure map values within the source aperture and the summed exposure map values in the local background region. This is similar to scaling by the relative sizes of the source aperture and background region, except this method accounts for variations in sensitivity due to chip gaps and edges, and HRMA mirror effects. Our simulations have shown that this method is both much faster and more accurate than measuring the local background using thousands of randomly placed apertures, as would be adopted in a Monte-Carlo approach.

For each source, the encircled-energy fraction was calculated using a tabular parameterization of the *Chandra* PSF, provided by the CXC, that gives the radius of a circular aperture for a given off-axis angle, photon energy, encircled-energy fraction, and azimuthal angle.<sup>6</sup> Using our desired aperture size, mean photon energy, and the sources' off-axis angles from the exposure-weighted mean aimpoints given by Alexander et al. (2003), we interpolated the HRMA FITS table to obtain the encircled-energy fraction for each source. Since the individual images used in the CDF-N and CDF-S mosaics were taken at a variety of roll angles, we removed the small azimuthal dependence by averaging the PSF parameterization over all azimuthal angles.

To calculate the total X-ray flux for all of the stacked sources, the total background-subtracted source counts (in photons) was divided by the sum of the mean exposure-map value within each extraction aperture (in  $\text{cm}^2\text{ s}$ ) to obtain the total photon flux for the stacked sources. This value was divided by the mean encircled-energy fraction, weighted by the mean exposure-map value for each source, and converted to energy flux by assuming a power-law spectrum with  $\Gamma = 1.4$  and correcting for Galactic absorption using the X-ray opacity table of Morrison & McCammon (1983) and the exposure-weighted mean Galactic column density ( $N_{\text{H}} = 1.16 \times 10^{20}\text{ cm}^{-2}$ ).

In Table 1, we show the stacking results for the 638 MIPS sources that lay within  $6'$  of the exposure-weighted

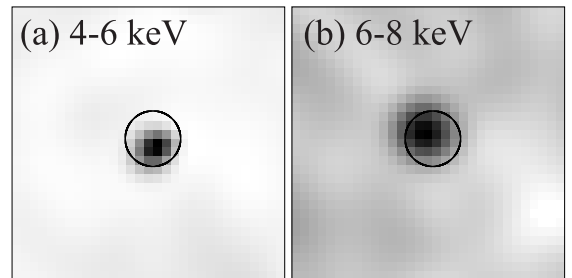


FIG. 2.— (a) Stacked, adaptively smoothed, 4–6 keV X-ray thumbnail for the 638 MIPS-selected AGN candidates. Adaptive smoothing was performed using the *csmooth* algorithm in CIAO. The  $3''$  diameter aperture used for source photometry is shown. (b) Stacked, adaptively smoothed 6–8 keV X-ray thumbnail.

<sup>5</sup> Available at <http://ssc.spitzer.caltech.edu/legacy/goodshistory.html>.

<sup>6</sup> Available at [http://cxc.harvard.edu/cal/Hrma/psf/ECF/hrmaD1996-12-20hrca\\_ecf\\_N0002.fits](http://cxc.harvard.edu/cal/Hrma/psf/ECF/hrmaD1996-12-20hrca_ecf_N0002.fits).

TABLE 1  
RESULTS OF X-RAY STACKING ANALYSIS OF MIPS SOURCES

Energy Band [keV] [1]	Total Counts [counts] [2]	Mean Background <sup>a</sup> [counts] [3]	Exposure Map (mean) [cm <sup>2</sup> s] [4]	Encircled Energy Fraction <sup>b</sup> [5]	Area <sup>c</sup> [deg <sup>2</sup> ] [6]	Total Intensity [ergs cm <sup>-2</sup> s <sup>-1</sup> deg <sup>-2</sup> ] [7]	% of CXB <sup>d</sup> [8]	S/N [σ] [9]
Standard <i>Chandra</i> X-ray bands								
0.5–8.0	6857.2 ± 82.8	4698.9 ± 6.2	$3.86 \times 10^8$	0.556	$5.676 \times 10^{-2}$	$(5.50 \pm 0.21) \times 10^{-13}$	$2.35 \pm 0.09$	26.0
0.5–2.0	2904.6 ± 53.9	1429.8 ± 3.4	$3.85 \times 10^8$	0.614	$5.930 \times 10^{-2}$	$(1.64 \pm 0.06) \times 10^{-13}$	$2.16 \pm 0.08$	27.3
2.0–8.0	3952.6 ± 62.9	3269.1 ± 5.2	$3.95 \times 10^8$	0.542	$5.559 \times 10^{-2}$	$(4.22 \pm 0.34) \times 10^{-13}$	$2.43 \pm 0.20$	10.8
Narrow X-ray bands								
0.5–1.0	1202.3 ± 34.7	679.2 ± 2.4	$2.50 \times 10^8$	0.624	$5.950 \times 10^{-2}$	$(0.60 \pm 0.04) \times 10^{-13}$	$1.99 \pm 0.13$	15.0
1.0–2.0	1702.4 ± 41.3	750.5 ± 2.5	$6.94 \times 10^8$	0.610	$5.920 \times 10^{-2}$	$(0.85 \pm 0.04) \times 10^{-13}$	$1.86 \pm 0.09$	23.0
2.0–4.0	1491.7 ± 38.6	1088.5 ± 3.0	$4.10 \times 10^8$	0.578	$5.826 \times 10^{-2}$	$(1.36 \pm 0.13) \times 10^{-13}$	$1.96 \pm 0.19$	10.4
4.0–6.0	1089.9 ± 33.0	927.8 ± 2.8	$4.32 \times 10^8$	0.544	$5.588 \times 10^{-2}$	$(0.97 \pm 0.20) \times 10^{-13}$	$1.73 \pm 0.36$	4.9
6.0–8.0	1371.0 ± 37.0	1252.3 ± 3.2	$1.69 \times 10^8$	0.504	$5.463 \times 10^{-2}$	$(2.83 \pm 0.89) \times 10^{-13}$	$5.79 \pm 1.82$	3.2

<sup>a</sup>The small error bars for the mean background result from the much larger area used to calculate this value, relative to the size of the extraction aperture.

<sup>b</sup>This is the mean encircled-energy fraction weighted by the exposure map values of the sources.

<sup>c</sup>This is the total area within  $6'$  of the CDF-N and -S aimpoints, corrected for the masked areas within  $2 \times 90\%$  encircled energy of the known X-ray sources.

<sup>d</sup>Assuming the CXB normalization of Hickox & Markevitch (2006). The CXB fraction is 11% higher assuming the normalization value measured by Revnivtsev et al. (2005) and 6% lower using the value from De Luca & Molendi (2004).

mean aimpoints of the CDF-N or the CDF-S, and were outside  $2 \times$  the radius of the 90% encircled-energy fraction of the X-ray sources in the Alexander et al. (2003) main and supplementary catalogs to avoid contamination from known X-ray sources. The X-ray stacking was performed in the three standard *Chandra* bands, the full (0.5–8.0 keV), soft (0.5–2 keV), and hard (2–8 keV) bands, as well as five narrower, non-overlapping X-ray bands.

From Table 1, the X-ray undetected MIPS source population makes up about 2% of the total CXB intensity below 6 keV. The resolved fraction of the CXB increases to  $\sim 6\%$  for the hardest X-ray energy band analyzed here. This is the first time that a statistically significant, stacked 6–8 keV signal has been found for an X-ray undetected population of sources. X-ray stacking analyses were used to measure the contribution of the optical GOODS sources to the CXB, but no significant 6–8 keV signal was found (Worsley et al. 2006). To verify the authenticity of the  $3.2\sigma$  detection in the 6–8 keV energy band, we extracted thumbnail X-ray images centered on each X-ray undetected MIPS source and coadded them. In Figure 2, we show the resulting  $15'' \times 15''$  stacked X-ray thumbnail for both the (a) 4–6 keV and (b) 6–8 keV bands with our  $3''$  diameter aperture overlaid (black circle). It is clear from these smoothed images that there is a significant stacked X-ray signal within our extraction aperture for both X-ray bands ( $p = 6.9 \times 10^{-4}$  in the 6–8 keV band, assuming a one-tailed Gaussian distribution). Our  $3''$  aperture was chosen to maximize the stacked signal within the aperture while minimizing the background signal. While the peak of the stacked X-ray image is not precisely centered within our aperture, using a larger aperture does not increase the measured S/N for the stacked 6–8 keV signal.

While we detect a significant 6–8 keV X-ray signal for the stacked, X-ray-undetected MIPS population we do not know how this low-level X-ray flux is distributed among the sources. Is the stacked 6–8 keV signal dominated by a small number of bright  $24\mu\text{m}$  sources, as one might suspect from Figure 1? To examine the importance of infrared flux on our X-ray stacking analysis, we break down our earlier stacking results by performing stacking as a function of limiting  $24\mu\text{m}$  flux. In Figure 3, we show the resolved fraction of the CXB,

the signal-to-noise (S/N), and the number of sources stacked as a function of limiting  $24\mu\text{m}$  flux. Overall, it appears that the S/N of our stacked X-ray signal does gradually increase as we include the X-ray flux from fainter MIPS sources, which suggests that the stacked X-ray signal is not dominated by a small number of bright  $24\mu\text{m}$  sources.

#### 4. DISCUSSION AND CONCLUSIONS

We present in this Letter results from an X-ray stacking analysis of the X-ray-undetected  $24\mu\text{m}$  *Spitzer* MIPS sources

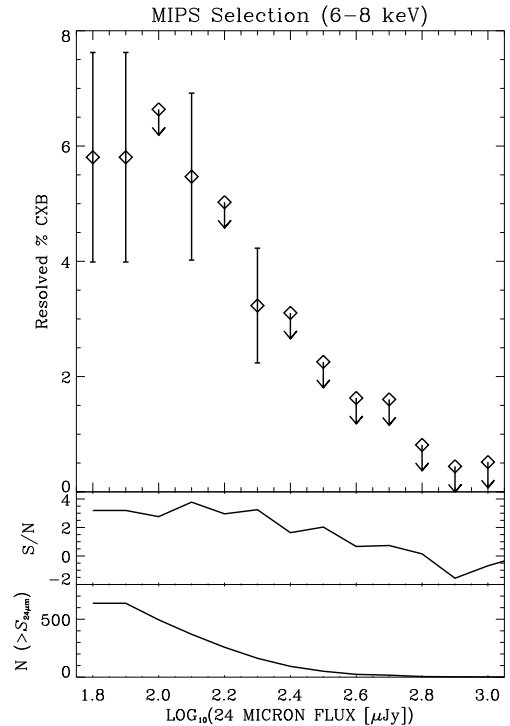


FIG. 3.— The total resolved 6–8 keV CXB fraction, the signal-to-noise of the stacked X-ray signal, and the total number of stacked sources as a function of  $24\mu\text{m}$  flux assuming the CXB normalization of Hickox & Markevitch (2006). Error bars ( $1\sigma$ ) are shown for stacked sources that have  $S/N > 3$ , and  $3\sigma$  upper limits are given for the stacked sources that are not significantly detected.

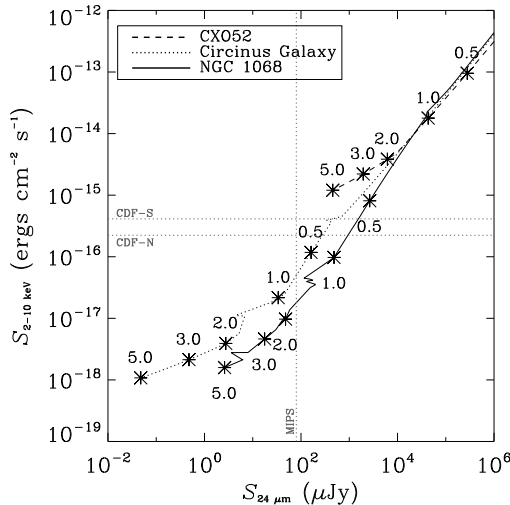


FIG. 4.— The redshift evolution of the observed-frame 2–10 keV flux and  $24\mu\text{m}$  flux density for three obscured AGNs, CXO52 (Stern et al. 2002, dashed curve), NGC 1068 (solid curve), and the Circinus galaxy (dotted curve). The two dotted horizontal lines and one dotted vertical line denote the average flux limits for the 2 Ms CDF-N, 1 Ms CDF-S, and the GOODS MIPS catalogues, respectively.

using the GOODS catalogs and the *Chandra* Deep Fields. We find, for the first time, a significant stacked X-ray signal ( $3.2\sigma$ ) in the 6–8 keV band for an X-ray-undetected, AGN-candidate sample, suggesting that at least some of these sources harbor heavily obscured AGNs. Approximately 12% of the unresolved fraction ( $\sim 50\%$ ; Worsley et al. 2005) of the 6–8 keV CXB can be attributed to these sources. The stacked 0.5–8 keV spectrum has a power-law photon index of  $\Gamma = 1.44 \pm 0.07$ , consistent with the slope of the CXB (Hickox & Markevitch 2006). The slope of the stacked X-ray spectrum hardens with increasing X-ray energy, suggesting that the flux from obscured AGNs dominates the stacked spectrum at high X-ray energies.

We found evidence that there exist mid-IR-bright, heavily obscured AGNs that are not individually detected in the X-ray band, but we know little about the general properties of these sources. By examining how the X-ray to  $24\mu\text{m}$  flux relation for AGNs evolves with redshift, we can infer the AGN types that are detected in this mid-IR catalog. In Figure 4, we examine the evolution of the X-ray to  $24\mu\text{m}$  flux relation for obscured AGNs using the observed SEDs of three obscured AGNs: the luminous, Type 2 quasar CXO52 (distant Compton-thin, obscured QSO;  $L_{2-10 \text{ keV}} = 3.3 \times 10^{44} \text{ ergs s}^{-1}$ , intrinsic; Stern et al. 2002), NGC 1068 (extreme Compton-thick, luminous AGN;  $L_{2-10 \text{ keV}} \sim 10^{43} - 10^{44} \text{ ergs s}^{-1}$ , intrinsic; Cappi et al. 2006); and the Circinus Galaxy

(Compton-thick, moderate-luminosity AGN;  $L_{2-10 \text{ keV}} \sim 10^{42} \text{ ergs s}^{-1}$ , intrinsic; Matt et al. 1999). This is similar to Figure 1 of Martínez-Sansigre et al. (2006), except here we utilize the observed SEDs of known obscured AGNs instead of using theoretical models. The rest-frame X-ray and IR fluxes were calculated by interpolating the SEDs provided by Stern et al. (2002) for CXO52, and the NASA/IPAC Extragalactic Database (NED) for NGC 1068 and the Circinus Galaxy.

From Figure 4 it is apparent that a luminous, significantly obscured AGN such as CXO52 would be detected in both the GOODS MIPS catalog and the deep X-ray surveys, even at  $z > 5$ , and would thus would not contribute to the unresolved portion of the CXB. Even if this source were Compton thick, it would easily be detected at  $24\mu\text{m}$  and would be included in our X-ray stacking analysis. Given the small fraction of the CXB that we resolve at 6–8 keV, the unresolved CXB at these energies *cannot* be attributed to a population of luminous, heavily obscured, “Type 2” Quasars at any redshift (unless Compton-thick QSOs are significantly fainter at  $24\mu\text{m}$  than their less obscured counterparts). In addition, it is apparent that heavily obscured, low-luminosity Seyfert 2s without significant star-formation can be detected in the MIPS band at  $z < 0.8$ , but fall below the GOODS detection threshold at higher redshifts. This suggests that the unresolved 6–8 keV CXB is not emanating primarily from a population of low-luminosity, low-redshift AGNs but could be from a population of low-luminosity,  $z > 0.8$  AGNs. At these low  $24\mu\text{m}$  fluxes it is difficult to separate AGNs from dusty starburst galaxies, which makes stacking analyses problematic due to the increased background signal in the 6–8 keV band from obscured starbursts.

The average 0.5–2 keV flux for our MIPS-selected AGNs is  $S_{0.5-2 \text{ keV}} \simeq 5.4 \times 10^{-18} \text{ ergs cm}^{-2} \text{ s}^{-1}$ , a factor of  $\sim 4.6$  lower than the flux limit of the 2 Ms CDF-N (Alexander et al. 2003). Deeper X-ray observations will help to improve significantly the S/N of the stacked X-ray signal and will greatly improve our measurements of the 6–8 keV CXB from these sources. In addition, if it is possible to separate better the obscured starbursts from the infrared-selected AGN candidates, the significance of the stacked X-ray detections should improve. We plan to address additional infrared AGN selection techniques in a subsequent paper (Steffen et al. 2007).

We gratefully acknowledge support from CXC grant GO4-5157A (A. T. S., W. N. B., B. D. L.), SAO grant AR6-7012X (A. T. S.), JPL grant 1278940 (A. T. S.), NASA LTSA grant NAG5-13035 (W. N. B.), the Royal Society (D. M. A), and JPL grant 1268000 (S. C. G.).

*Facilities:* CXO (ACIS), *Spitzer* (MIPS)

## REFERENCES

- Alexander, D. M., et al. 2003, *AJ*, 126, 539  
 Alonso-Herrero, A., et al. 2006, *ApJ*, 640, 167  
 Antonucci, R. 1993, *ARA&A*, 31, 473  
 Barger, A. J., et al. 2003, *AJ*, 126, 632  
 Bauer, F. E., et al. 2004, *AJ*, 128, 2048  
 Cappi, M., et al. 2006, *A&A*, 446, 459  
 Comastri, A., Setti, G., Zamorani, G., & Hasinger, G. 1995, *A&A*, 296, 1  
 De Luca, A. & Molendi, S. 2004, *A&A*, 419, 837  
 Dickinson, M. & GOODS Team 2005, American Astronomical Society Meeting Abstracts, 207  
 Donley, J. L., et al. 2007, *ApJ*, 660, 167  
 Fazio, G. G., et al. 2004, *ApJS*, 154, 10  
 Giacconi, R., et al. 2002, *ApJS*, 139, 369  
 Gilli, R., Comastri, A., & Hasinger, G. 2007, *A&A*, 463, 79  
 Hickox, R. C. & Markevitch, M. 2006, *ApJ*, 645, 95  
 Lacy, M., et al. 2004, *ApJS*, 154, 166  
 Laurent, O., et al. 2000, *A&A*, 359, 887  
 Lutz, D., Maiolino, R., Spoon, H. W. W., & Moorwood, A. F. M. 2004, *A&A*, 418, 465  
 Martínez-Sansigre, A., et al. 2006, *MNRAS*, 370, 1479  
 Matt, G., et al. 1999, *A&A*, 341, L39  
 Morrison, R. & McCammon, D. 1983, *ApJ*, 270, 119  
 Revnivtsev, M., Gilfanov, M., Jahoda, K., & Sunyaev, R. 2005, *A&A*, 444, 381  
 Rieke, G. H., et al. 2004, *ApJS*, 154, 25  
 Steffen, A. T., et al. 2004, *AJ*, 128, 1483

- Steffen, A. T., et al. 2007, in prep  
Stern, D., et al. 2002, ApJ, 568, 71  
Stern, D., et al. 2005, ApJ, 631, 163  
Szokoly, G. P., et al. 2004, ApJS, 155, 271  
Worsley, M. A., et al. 2004, MNRAS, 352, L28  
Worsley, M. A., et al. 2005, MNRAS, 357, 1281  
Worsley, M. A., et al. 2006, MNRAS, 368, 1735